Hindawi
Journal of Nanomaterials
Volume 2018, Article ID 5348016, 15 pages
https://doi.org/10.1155/2018/5348016

Research Article

Simultaneous Voltammetric Determination of Ascorbic Acid, Paracetamol, and Caffeine Using Electrochemically Reduced Graphene-Oxide-Modified Electrode

Nguyen Hai Phong, Tran Thanh Tam Toan, Mai Xuan Tinh, Tran Ngoc Tuyen, Tran Xuan Mau, and Dinh Quang Khieu

HU-University of Sciences, Hue 530000, Vietnam

Correspondence should be addressed to Dinh Quang Khieu; dqkhieu@hueuni.edu.vn

Received 7 March 2018; Revised 17 May 2018; Accepted 10 June 2018; Published 27 August 2018

Academic Editor: Jesús I. Valcarcel

In the present paper, graphene oxide was directly electrodeposited by means of cyclic voltammetric techniques on the glassy-carbon electrode (GCE) to obtain a reduced graphene-oxide-modified electrode (ErGO/GCE). Cyclic voltammetry (CV) and differential pulse anodic stripping voltammetry (DP-ASV) had been utilized to study the electrochemical behavior of ErGO/GCE toward ascorbic acid (AA), paracetamol (PA), and caffeine (CA). Differential pulse voltammetry results show that AA, PA, and CA could be detected selectively and sensitively on ErGO/GCE with peak-to-peak separation of 312 mV and 756 mV for AA–PA and PA–CA, respectively. The factors affecting the voltammetric signals such as pH, scan rate, and interferents were addressed. The results reveal that the ErGO/GCE-modified electrode exhibits excellent electrochemical activity in the oxidation of PA, CA, and AA. The detection limits are 0.36 μM, 0.25 μM, and 0.23 μM for AA, PA and CA, respectively, suggesting that the ErGO/GCE can be utilized with high sensitivity and selectivity for the simultaneous determination of these compounds. Finally, the proposed method was successfully used to determine AA, PA, and CA in pharmaceutical preparations.

1. Introduction

Ascorbic acid (AA), a vitamin commonly present in many biological systems and in multivitamin formulations, is widely employed to provide an adequate dietary intake and as an antioxidant [1, 2]. Its overdoses may cause gastrointestinal discomfort, headache, trouble sleeping, and flushing of the skin [3]. These drugs are often combined in two or three types to increase the possibility of therapy. Paracetamol or acetaminophen (N-acetyl-p-aminophenol or paracetamol (PA)) is an antipyretic and analgesic drug commonly used against arthritis, muscle aches, and fevers [4]. A high amount of PA can cause the accumulation of toxic metabolites, leading to severe and sometime fatal hepatotoxicity and nephrotoxicity [5]. Caffeine (1,3,7-trimethylxanthine (CA)) is an alkaloid component present in natural products such as coca cola, coffee, and tea leaves [6]. It is known to have many pharmacological effects including as a diuretic, cardiac stimulant, and stimulant of the central nervous system [6, 7]. Caffeine is employed in combination with ergotamine in migraine treatment [8]. However, large doses of caffeine can cause nausea, abdominal pain, nervousness and seizures [9], and mutation effects such as inhibition of DNA [10]. Therefore, it is very important to determine the amount of these compounds sensitively, simultaneously, accurately, and fast.

Several analytical methods for individual or simultaneous determination of AA, PA, and CA have been reported in the literature such as spectrofluorometry [11, 12], chromatography [13, 14], spectrophotometry [15, 16], capillary zone electrophoresis [17, 18], and electrochemistry [19–22], among which electrochemical methods based on modified electrodes have fascinated many researchers due to their simplicity, high sensitivity, and low cost. However, one major obstacle is that the oxidation peaks of AA and PA are almost overlapping on traditional electrodes, which

make their simultaneous determination highly difficult [23, 24]. For this reason, it is necessary to prepare modified electrodes that can be employed for simultaneous detection of these compounds.

Graphene consists of a flat monolayer of sp^2-carbon atoms bonded and arranged in a honeycomb lattice. It has attracted extensive interest because of its unique properties including its ideal two-dimensional structure [25], electronic properties [26], mechanical properties [27], and thermal properties [28]. Furthermore, graphene oxide (GO) and reduced graphene oxide (rGO) have also been employed in modified electrodes. rGO has better conductivity than GO and restores the unique properties found in the pristine graphene. Some reports are related to the application of rGO-based materials in electrochemistry [27–29]. Various methods including chemical reduction [30, 31], thermal reduction [32, 33], photocatalytic reduction [34, 35], and electrochemical reduction [36] have been used to prepare rGO. The electrochemical reduction of GO is a relatively simple, economical, fast, and green method. This method could restore some of the original properties of pristine graphene and exploit new functionalities of rGO, along with other nanoparticles or compounds [36]. rGO produced using this method is known as electrochemically reduced graphene oxide (ErGO). To the best of our knowledge, the simultaneous voltammetric determination of AA, PA, and CA using an ErGO-modified electrode has not been reported.

In the present paper, an electrode modified with electrochemically reduced graphene oxide is demonstrated. The obtained electrode was used for the simultaneous determination of AA, PA, and CA by means of the DP-ASV method.

2. Experimental

2.1. Materials. Graphite powder, potassium permanganate ($KMnO_4$), sodium acetate ($NaCH_3COO$), sodium citrate ($Na_3C_6H_5O_7$), sodium dihydrogen phosphate (NaH_2PO_4), sodium hydrogen phosphate (Na_2HPO_4), acetic acid (CH_3COOH), ascorbic acid ($C_6H_8O_6$), citric acid ($C_6H_8O_7$), boric acid (H_3BO_3), ammonia solution (NH_4OH, 25%), paracetamol ($C_8H_9NO_2$, 99%), caffeine ($C_{18}H_{10}N_4O_2$, 98.5%), and ascorbic acid ($C_8H_6O_6$, 99.7%) were supplied from Merck company (Germany). Sodium nitrate ($NaNO_3$), ethanol (C_2H_5OH), hydroperoxide (H_2O_2, 30%), and potassium hydroxide (KOH) were supplied by Daejung company (Korea). Phosphate-buffered solution (PBS) with pH 6 was prepared from 1 M NaH_2PO_4 and 1 M Na_2HPO_4. Britton–Robinson buffer solutions (B–RBS) in the range of pH from 2 to 6 were prepared from 0.5 M H_3BO_3, 0.5 M H_3PO_4, and 0.5 M CH_3COOH. The desired pH 6 buffer was adjusted using 1 M KOH or 1 M H_3PO_4 solutions.

2.2. Methods. X-ray diffraction measurements were performed on a D8 Advance (Bruker, Germany) with CuK_α radiation ($\lambda = 0.1514$ nm). Fourier transformation infrared analyses were recorded on a Shimadzu IRPrestige-21 (Japan). Raman spectra were obtained using XploRA, HORIBA (Japan), 532 nm YAG Laser. A CPA-HH5 Computerized Polarography Analyzer (Vietnam) was used for voltammetry measurements. All measurements were performed in a cell with three electrodes: a glassy-carbon electrode (GCE) with a diameter of 2.8 ± 0.1 mm used for formatting the modified electrode as the working electrode, an Ag/AgCl/3 M KCl as a reference electrode, and a platinum wire as an auxiliary electrode. All measurements were performed at ambient temperature.

Table 1: Factors and their levels in full factorial design.

Factor	Level		
	Low (−1)	Medium (0)	High (+1)
Amount of GO (mg)	2	6	10
Number of cycles	4	8	12
Scan rate ($V \cdot s^{-1}$)	0.01	0.08	0.15

The HPLC (high-performance liquid chromatography) method was carried out to analyse AA, PA, and CA for the sake of comparison. Chromatographic determinations were performed in a Shimadzu 2030 HPLC system. The chromatographic conditions are as follows: UV detector ($\lambda = 275$ nm), flow rate set at 2.0 mL·min^{-1} with 10 μL as the injection volume, and column temperature set at $45^\circ C \pm 1^\circ C$. All the calculations concerning the quantitative analysis were performed with external standardization by measuring the peak areas of the chromatograms.

2.3. Preparation of ErGO/GCE. Graphene oxide was prepared using the modified Hummers process [36, 37]. Reduced graphene oxide was directly prepared on GCE by means of electrochemical reduction. Graphene oxide was applied by cyclic voltammetry with a potential range from 0 V to −1.5 V in the 0.2 M phosphate buffer of pH 7.

In this study, the effect of the amount of GO (z_1), number of cycles (z_2), and scanning rate (z_3) on the peak current of ErGO/GCE was studied using the Box–Behnken design [38–40]. The number of experiments (N) required for the development of this design is defined as $N = 2 \cdot k \cdot (k-1) + C_0$, where k is the number of factors ($k = 3$) and C_0 is the number of replicates at the center point ($C_0 = 3$) [41]. Thus, a total of 15 runs were carried out for optimizing these three variables. Each independent variable was considered at three levels: low, medium, and high, coded as −1, 0, and +1, respectively (Table 1). The center points were used for the determination of error. Based on the experimental data, a second-order polynomial model was obtained, which correlates the relationship between the response and the studied variables. The relationship could be expressed in

$$y = b_0 + b_1 \cdot z_1 + b_2 \cdot z_2 + b_3 \cdot z_3 + b_{11} \cdot {z_1}^2 + b_{22} \cdot {z_2}^2 + b_{33} \cdot {z_3}^2 + b_{12} \cdot z_1 \cdot z_2 + b_{13} \cdot z_1 \cdot z_3 + b_{23} \cdot z_2 \cdot z_3, \quad (1)$$

where y is the predicted response value (peak current (I_p)); z_1, z_2, and z_3 are independent variables; b_0 is the intercept term; b_1, b_2, and b_3 are linear coefficients; b_{12}, b_{13}, and b_{23}

are cross-product coefficients; and b_{11}, b_{22}, and b_{33} are quadratic-term coefficients. All the coefficients of the second polynomial model and the response obtained from the experimental design were subjected to multiple nonlinear regression analyses. The empirical relationships between the response (y) and the tested variables were obtained using Minitab version 16.

2.4. Pharmaceutical Preparation. Panadol Extra (Sanofi-Synthelabo company, Vietnam), Hapacol Extra (DHG Pharma company, Vietnam), Tatanol (Pymepharco company, Vietnam), Effe-Paracetamol (Pymepharco company, Vietnam), Ameflu C (OPV company, Vietnam), and Efferalgan Vitamin C (Laboratoires UPSA company, France) were employed in this study. Ten tablets of each analysed pharmaceutical preparation were weighed and finely ground in a mortar. An exact amount of the powder was weighed and transferred to a 100 mL calibrated flask, which was filled to the volume with the 0.2 M B–R buffer solution of pH 3.2. The standard addition method was used for determining the pharmaceutical formulations.

3. Result and Discussion

3.1. The Preparation of ErGO/GCE Based on the Box–Behnken Design. In the present study, the optimum levels of the variables including the amount of GO (z_1), number of cycles (z_2), and scan rate (z_3) were studied with the Box–Behnken design.

Based on the experimental data (Table S1, Table S2, and Table S3), three equations of the experimental design were established using Minitab 16 ((2), (3), and (4)). They correlate the relationship between the peak current of AA, PA, and CA and the three variables.

$$\begin{aligned} I_{\mathrm{p,AA}} &= 2.42 + 0.08 \cdot z_1 + 0.10 \cdot z_2 - 0.13 \cdot z_3 - 0.25 \cdot {z_1}^2 \\ &\quad - 0.16 \cdot {z_2}^2 - 0.13 \cdot {z_3}^2 + 0.05 \cdot z_1 \cdot z_2 - 0.05 \cdot z_1 \cdot z_3 \\ &\quad - 0.01 \cdot z_2 \cdot z_3, \\ r &= 0.994, \end{aligned} \tag{2}$$

$$\begin{aligned} I_{\mathrm{p,PA}} &= 5.29 + 0.31 \cdot z_1 + 0.38 \cdot z_2 - 0.48 \cdot z_3 - 1.03 \cdot {z_1}^2 \\ &\quad - 0.68 \cdot {z_2}^2 - 0.56 \cdot {z_3}^2 + 0.23 \cdot z_1 \cdot z_2 - 0.22 \cdot z_1 \cdot z_3 \\ &\quad - 0.03 \cdot z_2 \cdot z_3, \\ r &= 0.972, \end{aligned} \tag{3}$$

$$\begin{aligned} I_{\mathrm{p,CA}} &= 3.95 + 0.28 \cdot z_1 + 0.37 \cdot z_2 - 0.44 \cdot z_3 - 0.86 \cdot {z_1}^2 \\ &\quad - 0.45 \cdot {z_2}^2 - 0.37 \cdot {z_3}^2 + 0.18 \cdot z_1 \cdot z_2 - 0.16 \cdot z_1 \cdot z_3 \\ &\quad - 0.06 \cdot z_2 \cdot z_3, \\ r &= 0.928. \end{aligned} \tag{4}$$

The coefficients corresponding to each factor in the linear and quadratic terms and their interactions in (2), (3), and (4) have the same sign. A minus sign suggests an antagonistic effect, whereas a plus sign indicates a synergistic effect. The absolute value of the coefficients determines the significance of the effect. Thus, the signs of the coefficients and their values indicate that those amounts of GO, number of cycles, and scan rate act in the same way on the peak current for AA, PA, and CA oxidation, but the level of importance is different. As seen in the equations, the amount of GO (z_1) and number of cycles (z_2) have a positive effect. This indicates that the intensity of the peak current can be improved when the value of these factors increase, whereas the increasing scan rate (z_3) reduces the peak current because the sign of z_3 is minus.

Since the peak current for AA oxidation is the lowest (Figure 1(b)), it was chosen for the optimization of the variables in the preparation of ErGO/GCE.

The obtained results through ANOVA (Table S4) show that most of the factors (z_1, z_2, z_3, ${z_1}^2$, ${z_2}^2$, ${z_3}^2$, $z_1 \cdot z_2$, and $z_1 \cdot z_3$) have the p value of less than 0.05, indicating that they are significant (this means that the amount of GO, number of cycles, scan rate, the interactions between the amount of GO and the number of cycles, and the amount of GO and scan rate significantly affect the peak current of AA). Only b_{23} has the p value of more than 0.05, and it will be removed from (2). Then, the reduced form of (2) is as follows:

$$\begin{aligned} I_{\mathrm{AA}} &= 2.42 + 0.08 \cdot z_1 + 0.10 \cdot z_2 - 0.13 \cdot z_3 - 0.25 \cdot {z_1}^2 \\ &\quad - 0.16 \cdot {z_2}^2 - 0.13 \cdot {z_3}^2 + 0.05 \cdot z_1 \cdot z_2 - 0.05 \cdot z_1 \cdot z_3. \end{aligned} \tag{5}$$

The analysis of variance is used to estimate the statistical significance of the model. The summary of the analysis of variance is shown in Table 2. If the p value is lower than 0.05, it means that the model is statistically significant. The fitness of the model equation was estimated according to the determination coefficient (R^2). The results show that the value of R^2 is 0.988. This means that the calculated model is able to explain 98.8% of the results (or of the variability of the response). This result also indicates a good agreement between the experimental and predicted values of the response. The p value for the "lack of fit" test is 0.856. This finding suggests that the model employed to fit the response variables is significant and adequate to describe the relationship between the response and the independent variables.

The profile for the predicted values and desirability option in the Minitab 16 is applied for the optimization process. Figure 1(a) presents the optimization plots of AA. The optimization shows the maximum I_{p} (2.49) obtained under the following conditions: amount of GO being 7.0 μg, number of cycles being 10, and scan rate being 0.04 V·s^{-1}. The reliability of this prediction was checked by carrying out three replicates under these optimal conditions. The experimental I_{p} for AA are 2.47, 2.47, and 2.49 (Figure 1(b)). The comparison by means of one-sample t-test shows that there

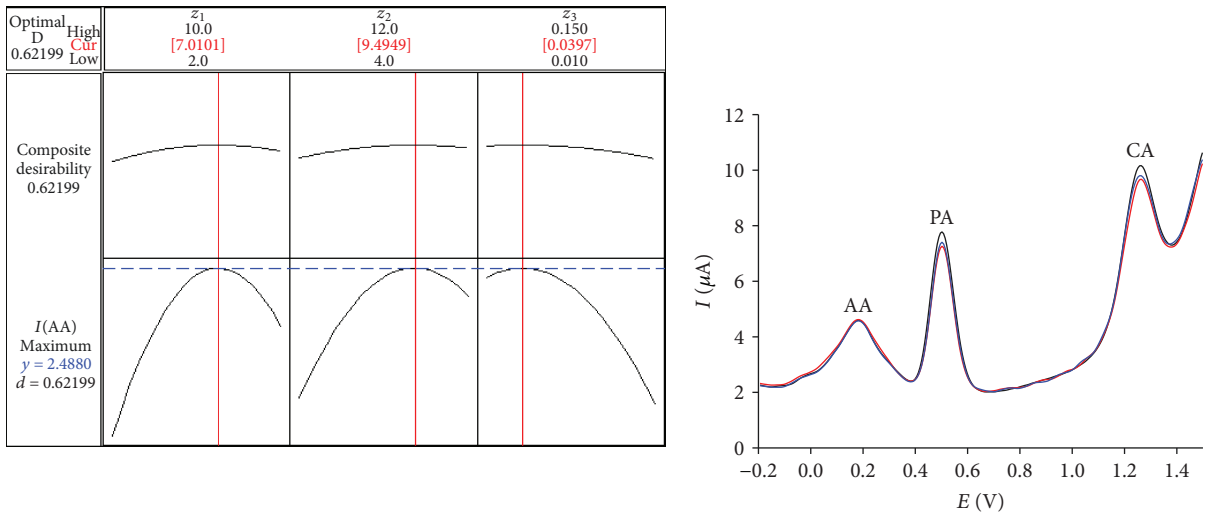

Figure 1: (a) Optimization plot for peak current of AA oxidation; (b) DP-ASV curves obtained at the ErGO/GCE prepared at optimization conditions ($C_{AA} = C_{PA} = C_{CA} = 1\,\mu$M in a 0.2 M B–R buffer solution of pH 3.2).

is no significant difference in the respective value presented by the model ($t(2) = -2$; $p = 0.184 > 0.05$). This demonstrates that the optimization is acceptable. These conditions were selected for the next experiments.

Figure 2(a) illustrates the electrochemical reduction of the GO by means of the CV technique. GO was drop cast on GCE under the optimal conditions (7.0 μg, 10 cycles, and 0.04 mV·s^{-1}). In aqueous solution, the film was reduced by potential cycling between 0 V and −1.5 V at pH 7. As seen in Figure 2(a), the first cycle shows a large cathodic peak current starting at around −1.23 V, and the reduction current observed could be related to the reduction of oxygen functional groups on GO. During the second cycle, the reduction current decreases significantly and vanishes after the third cycle. This observation is consistent with that of the previous papers [42, 43]. XRD measurements were used to study the phase of the obtained samples. Figure 2(b) shows the XRD patterns of graphite, GO, and ErGO. The characteristic diffraction peak of GO at 2θ of around 11.3° indicates that oxygen-containing functional groups on graphite sheets are formed, that is, the formation of GO [44, 45]. Peaks at around 26° could be attributed to the initial graphite indicating that the oxidation of graphite is incomplete. After being electrochemically reduced, the material does not show the peak at 11.3°, and the weak and broad reflection peak at 25.8° corresponds to the relative short-range-order structures in disordered stacked rGO [44], which indicates the successful reduction of GO.

The existence of oxygen-containing functional groups was confirmed by FT–IR (Figure 2(c)). The strong absorption band at 3417 cm^{-1} is attributed to ν_{OH} as the graphite was oxidized. The vibration bands at 1720 cm^{-1} and 1620 cm^{-1} can be responsible for $\nu_{C=O}$ of carbonyl and $\nu_{C=C}$ of aromatic rings, respectively. The absorption bands at 1051 cm^{-1} can be assigned to ν_{C-O} of alkoxy [36, 46]. The vibrational band at 1395 cm^{-1} can belong to ν_{COO}. The presence of the oxygen-containing functional groups again indicates the successful oxidation of graphite to graphite oxide.

Table 2: Analysis of variance for the fitted quadratic polynomial model of the preparation of ErGO/GCE.

Source	DF	SS	MS	p value
Regression	9	2.52569	0.280632	0.000
Residual	50	0.02975	0.000595	—
Lack of fit	3	0.00048	0.000160	0.856
Pure error	47	0.02927	0.000623	—

DF: degrees of freedom; SS: sum of squares; MS: mean of squares.

Raman spectroscopy is a useful technique for the characterization of the physicochemical properties of graphene. In general Raman spectroscopy, the G band contributes to the first-order scattering of the E_{2g} phonon of sp^2 C atoms (~1570 cm^{-1}) and the D band is attributed to a breathing mode of k-point photons of A_{1g} symmetry (~1350 cm^{-1}). At the same time, an increased I_D/I_G ratio arises from a lower degree of crystallinity in the graphitic materials. Two bands of the Raman spectra of GO and ErGO were observed at approximately 1352 and 1570 cm^{-1}, contributing to the D band and G band, respectively (Figure 2(d)). The intensity ratio of the D and G bands increased from 0.90 to 1.14 due to the electrochemical reduction, suggesting a decrease in the size of the in-plane sp^2 domains and the partially ordered crystal structure of graphene. These results provided more evidence for removing oxygen-containing functional groups from the surface of GO by means of electrochemical reduction [36, 46].

3.2. Electrochemical Behavior of ErGO-Based GCE. The CV experiments were conducted on bare GCE and ErGO/GCE

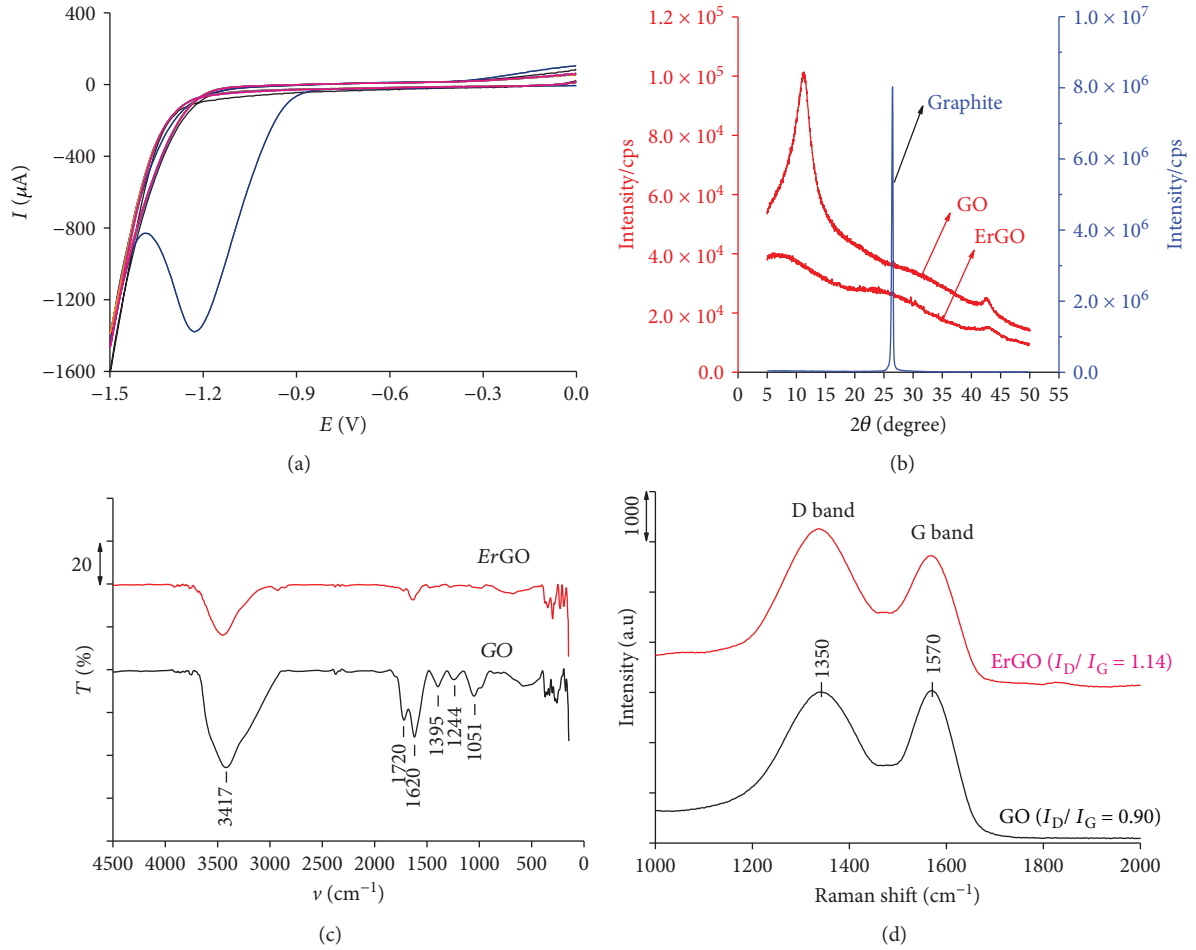

FIGURE 2: (a) CV curves of GO film in 0.2 M PBS (pH 7) at a scan rate of 0.04 $V \cdot s^{-1}$; (b) XRD patterns of graphite, GO, and ErGO; (c) FT–IR and (d) Raman spectra of GO and ErGO.

by using 1.0 mM $K_4Fe(CN)_6$ in 0.1 M KCl as a standard probe [47]. For the reversible process, the Randles–Sevcik formula in a simplified form (6) was employed to calculate the effective surface area of the GCE and modified GCE.

$$I_{pa} = \left(2.69 \cdot 10^5\right) \cdot n^{3/2} \cdot A \cdot {D_0}^{1/2} \cdot C \cdot \nu^{1/2}, \quad (6)$$

where I_{pa} refers to the anodic peak current, n is the number of electrons transferred, A is the effective surface area, D_0 is the diffusion coefficient, C is the concentration of $K_4Fe(CN)_6$, and ν is the scan rate.

For 1.0 mM $K_4Fe(CN)_6$ in 0.1 M KCl electrolyte, n is equal to 1 and D_0 is 7.6×10^{-6} $cm^2 \cdot s^{-1}$. Then, the effective surface area calculated from the slope of the plot of I_{pa} versus $\nu^{1/2}$ is 0.043 cm^2 and 0.050 cm^2 for GCE and ErGO/GCE, respectively (see Figure S1). This means that ErGO/GCE provided a larger effective surface than the bare GCE did.

The values of the heterogeneous electron transfer rate constant, k_{0obs}, were determined by means of the Nicholson method combined with the following equation: $\psi = k_{0obs} \cdot [\pi \cdot D \cdot n \cdot \nu \cdot F/(R \cdot T)]^{-1/2}$, where ψ is the kinetic parameter, D is the diffusion coefficient, n is the number of electrons involved in the process ($n = 1$), ν is the scan rate, F is the Faraday constant ($F = 96{,}480\ C \cdot mol^{-1}$), R is the universal gas constant ($R = 8.314\ J \cdot K^{-1} \cdot mol^{-1}$), and T is the temperature ($T = 298$ K) [47, 48]. The kinetic parameter, ψ, is calculated as a function of ΔE_P (peak-to-peak separation) at the set temperature (298 K) for a one-step, one-electron process with the transfer coefficient, α, equal to 0.5. The function of ψ (ΔE_P), which fits Nicholson's data for a practical usage, is given by $\psi = (-0.6288 + 0.0021 \cdot X)/(1 - 0.017 \cdot X)$ where $X = \Delta E_P$ is used to determine ψ as a function of ΔE_P from the experimentally recorded cyclic voltammetry. The values of k_{0obs} were obtained from the slope of the plot of ψ against $[\pi \cdot D \cdot n \cdot \nu \cdot F/(R \cdot T)]^{-1/2}$. The heterogeneous electron transfer rate constants for 1.0 mM $K_4Fe(CN)_6$ in 0.1 M KCl electrolyte were 16×10^{-6} for GCE and 3.7×10^{-6} $cm \cdot s^{-1}$ for ErGO/GRE (see Figure S2). The k_{0obs} for ErGO/GGE is lower than that for the bare GGE. This may be due to the electrode modification which increases the resistance of electrode.

The CV experiments were also performed on a modified GCE with and without ErGO in order to confirm its

electrochemical behavior for the detection of AA, PA, and CA (Figure 3). As can be seen in the figure, the current response on bare GCE and GO/GCE exhibits broad peaks, while the current response on ErGO/GCE provides defined peaks. The intensity of the anodic peak current (henceforth I_p) of AA, PA, and CA on ErGO/GCE was 59.17-, 72.78-, and 12.49-fold, respectively, compared with that on the bare GCE. The peaks of AA and PA are often overlapped, leading to difficulties in their simultaneous determination. It is worth noting that the peak-to-peak separation of 312 mV and 756 mV for AA–PA and CA–AA, respectively, was obtained on the ErGO, while it is not observed on bare GO or ErGO/GCE in this study. The favorable signal-promoting effect of the ErGO suggests that it could accelerate the electron transfer of the analytes and had a good electrocatalytic activity for the *redox* reaction of AA, PA, and CA. ErGO contains carboxyl groups and aromatic rings. The π–π stacking interaction between the aromatic rings of the analytes and ErGO is possibly responsible for the accumulation of AA, PA, and CA on the modified electrode. The process is illustrated in Scheme 1.

3.3. Effect of the pH. The effect of the pH on the voltammetric signals of AA, PA, and CA was studied in the pH range of 2.3 to 5.8 using the B–RBS (Figure 4(a)) with the CV method in order to estimate the relevant pH and also the ratio of electrons and protons participating in the voltammetric process on ErGO/GCE. As can be seen from Figure 4, the highest values of I_p for CA are at pH 3.2, while I_p for AA and PA decreases slightly as pH increases from 2.3 to 5.8. Therefore, pH = 3.0 ÷ 3.2, which is suitable for the analytes, was chosen for subsequent analytical experiments.

It was found that the oxidation peak potential (E_p) is dependent on pH. The potentials for AA, PA, and CA shift towards less positive values as the pH gradually increases, suggesting the involvement of protons in the oxidation reaction. Within the pH range 2.3–5.8, the linear regression equations for the oxidation peak potentials ($E_{p,AA}$, $E_{p,PA}$, and $E_{p,CA}$) and pH are expressed as follows:

$$\begin{aligned} E_{p,AA} &= 0.54 \pm 0.01 + (-0.054 \pm 0.002) \cdot \text{pH}, \\ r &= 0.997, \\ E_{p,PA} &= 0.87 \pm 0.03 + (-0.061 \pm 0.007) \cdot \text{pH}, \\ r &= 0.983, \\ E_{p,CA} &= 1.63 \pm 0.03 + (-0.049 \pm 0.008) \cdot \text{pH}, \\ r &= 0.966. \end{aligned} \quad (7)$$

The values of 0.054 V/pH for AA, 0.061 V/pH for PA, and 0.049 V/pH for CA are close to the Nernstian slope of 0.059 V/pH, indicating that the oxidation of AA, PA, and CA involves an equal number of electrons and protons.

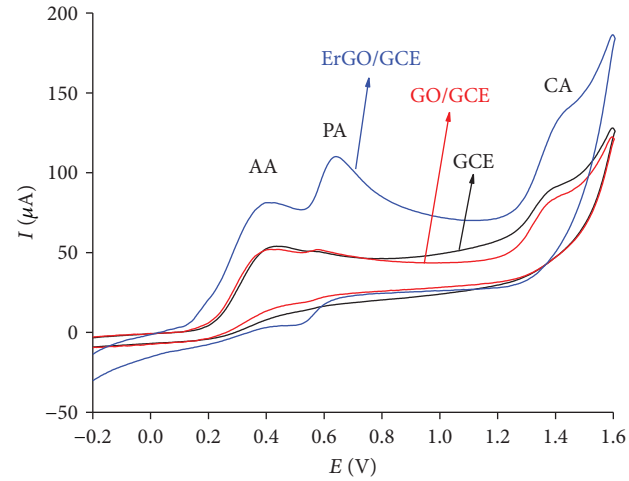

Figure 3: Cycles for AA, PA, and CA on bare GCE and GO/GCE and ErGO/GCE. ($C_{AA} = 100\,\mu$M; $C_{PA} = C_{CA} = 10\,\mu$M in 0.2 M B–RBS of pH 7; scan rate = 0.2 V · s^{-1}).

The mechanisms of PA [49] and AA [5] oxidation with two electrons and two protons are illustrated in Schemes 2(a) and 2(b). The CA oxidation on the electrode is believed to take place in two steps [50]. The first low step involves the oxidation of the C–8 to N–9 bonds and produces 1,3,7-trimethyluric acid with the involvement of two electrons and two protons. The second fast step is followed by 2e, 2H$^+$ oxidation to 4,5-dihydroxy-1,3,7-trimethyltetrahydro-1-H-purine-2,6,8-trione and 4,5-dihydroxy-1,7,9-trimethyltetrahydro-1-H-purine-2,6,8-trione (Scheme 2(c)). Since the first step is slow, it limits the rate of the reaction. Hence, the CA oxidation involves two electrons and two protons.

3.4. Effect of Scan Rate. The relationship between the voltammetric signal and the scan rate (denoted as ν) could give important information about the voltammetric mechanism. Hence, the relationships between on E_p, I_p, and ν were performed by cyclic voltammetry, as shown in Figure 5(a).

If the electrooxidation reaction is irreversible, the peak potential is independent of the scan rate. As can be seen from Figure 5(b), E_p seems to be independent of ν, and the peak potential shifts only slightly to a higher potential as the scan rate increases. It may, therefore, be concluded that electron transfers in the AA, PA, and CA electrooxidation are *quasi*-reversible. I_p increases with the increase in ν from 0.1 V·s^{-1} to 0.4 V·s^{-1} (Figure 5(c)), indicating that the electron transfer reaction involves a surface-confined process [46].

The plots of ln I_p versus ln ν were established to determine whether the electrooxidation reactions are controlled by adsorption or diffusion processes. If the plot of I_p versus ν is linear and the slope is close to 1, the electrooxidation reaction is an adsorption-controlled process. Otherwise, the slope is close to 0.5, then the process is controlled by the diffusion [51]. Natural logarithm I_p for AA, PA, and CA as a function of ln ν is expressed as follows:

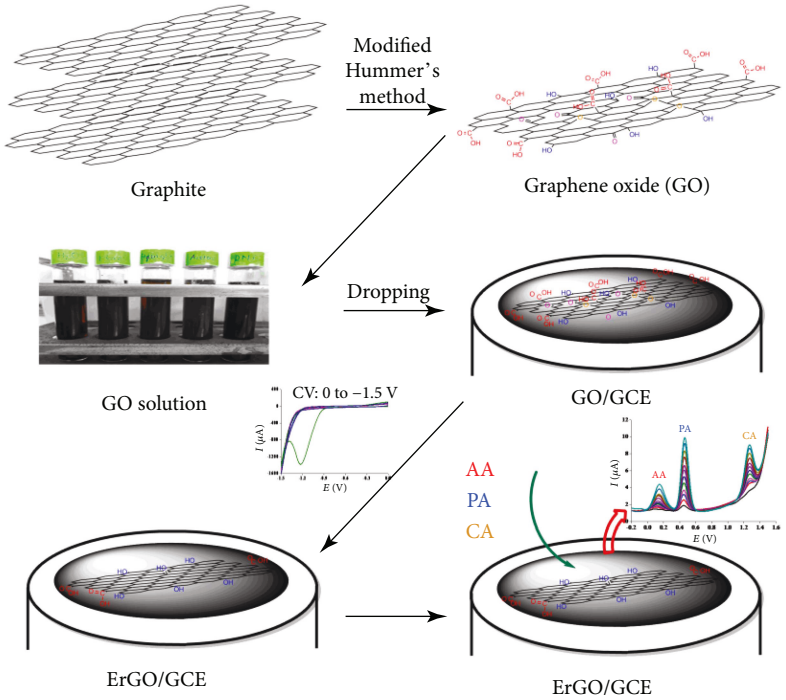

Scheme 1: Simultaneous voltammetric determination of AA, PA, and CA by means of electrochemically reduced graphene-oxide-modified electrode.

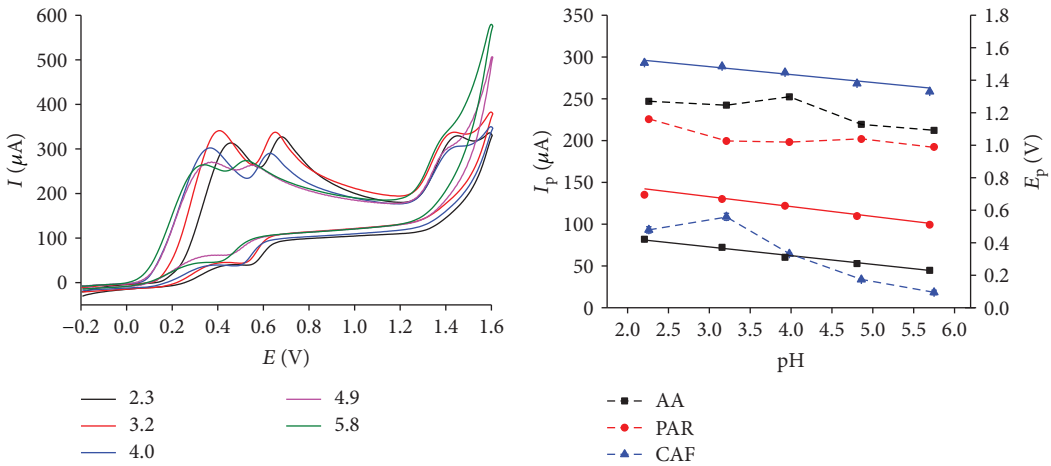

Figure 4: (a) CV curves at different pHs; (b) peak current I_p and peak potential E_p versus pH experimental condition. Volt scanning: −0.2 ÷ 1.6 V; scan rate: 0.2 V·s^{-1}; $C_{AA} = 100\,\mu$M; $C_{PA} = C_{CA} = 10\,\mu$M in 0.2 M B–RBS (pH = 2.3 ÷ 5.8).

$$\begin{aligned} \ln I_{p,AA} &= 6.18 \pm 0.02 + (0.70 \pm 0.03) \cdot \ln \nu, \\ r &= 0.995, \\ \ln I_{p,PA} &= 5.918 \pm 0.006 + (0.863 \pm 0.008) \cdot \ln \nu, \\ r &= 1.000, \\ \ln I_{p,CA} &= 4.50 \pm 0.06 + (0.64 \pm 0.08) \cdot \ln \nu, \\ r &= 0.960. \end{aligned} \tag{8}$$

The slope of plots for $\ln I_{p,AA}$, $\ln I_{p,PA}$, and $\ln I_{p,CA}$ against $\ln \nu$ (Figure 5(d)) are highly linear ($r = 0.960 \div 1.000$, $p < 0.001$) and 0.70, 0.863, and 0.64, respectively. The values of the slope are around 0.5 and 1. This indicates that AA, PA, and CA electrooxidations are diffusion-adsorption-controlled processes.

3.5. Effect of Pulse Amplitude, Accumulation Potential, and Time. The influence of accumulation potential and time on

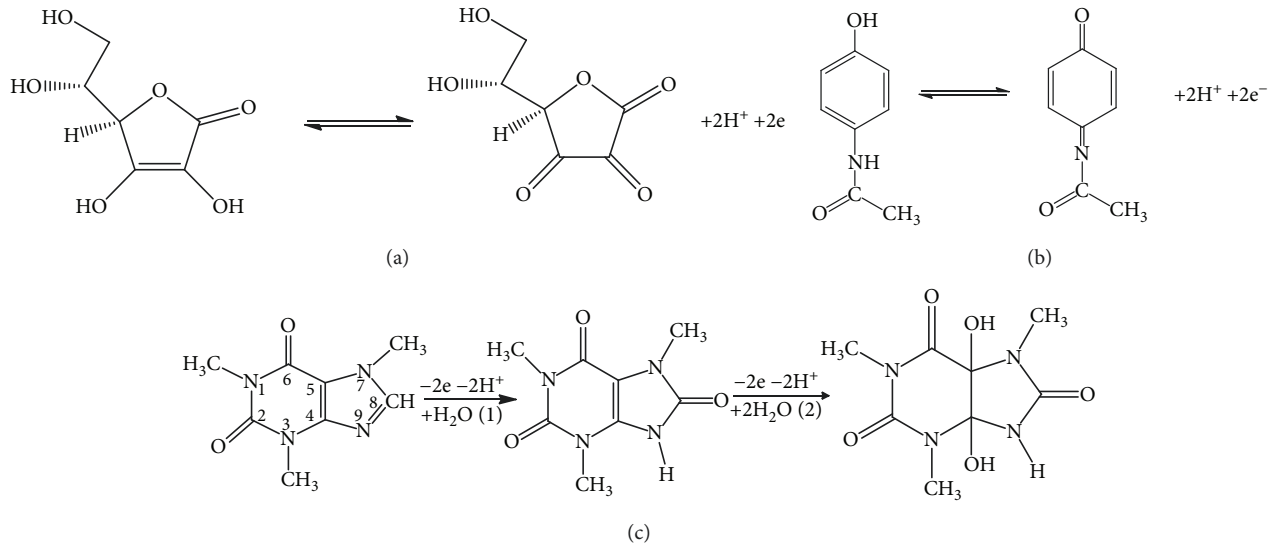

Scheme 2: Mechanisms of (a) AA oxidation, (b) PA oxidation, and (c) CA oxidation.

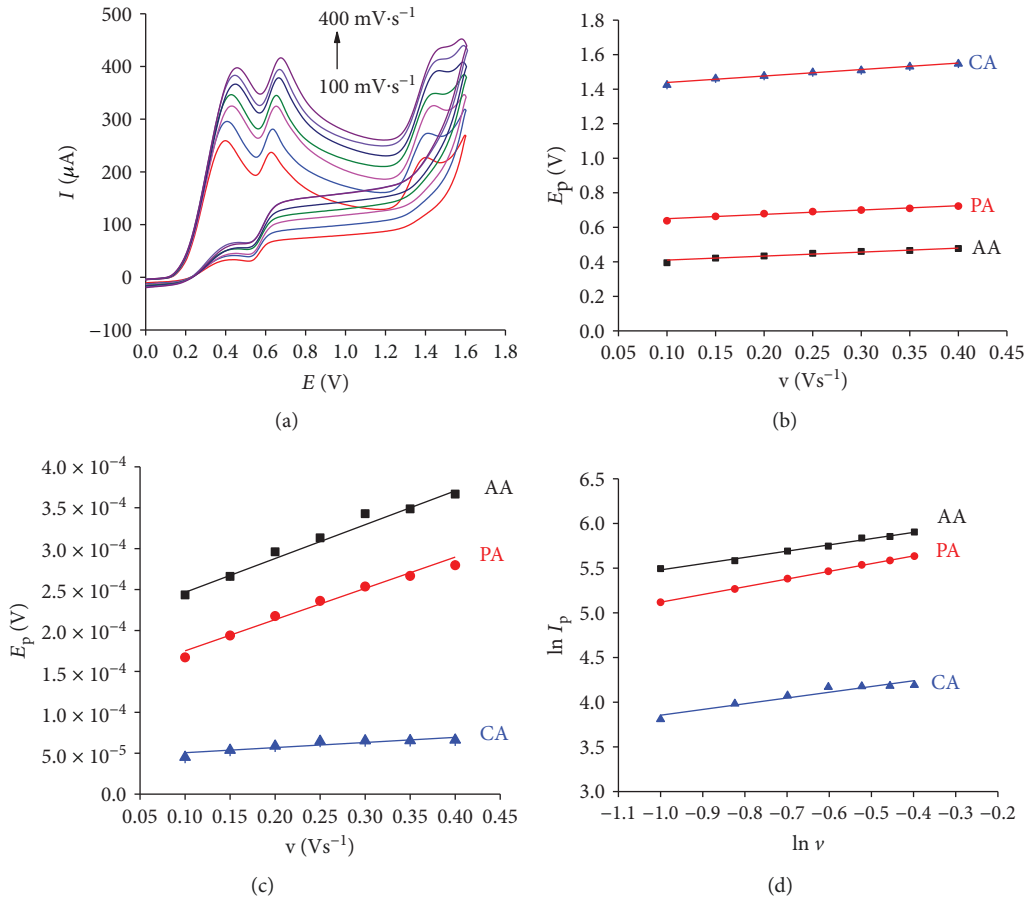

Figure 5: CV curves at different scan rates (a); linear plot of E_p versus ν (b); I_p versus ν (c); ln I_p versus ln ν (d); experimental conditions: volt scanning: −0.2 ÷ 1.6 V, $C_{AA} = 100\ \mu$M, and $C_{PA} = C_{CA} = 10\ \mu$M in 0.2 M B–RBS of pH 3.2.

the I_p of the analytes on ErGO/GCE was also investigated using the DP-ASV method in the range of −0.2 V to 0.3 V (Figures 6(a) and 6(b)).

As can be seen in Figure 6(a), $I_{p,PA}$ increases as the potential shifts positively from −0.2 V to 0.3 V but I_p of AA and CA decreases. The appropriate accumulation potential

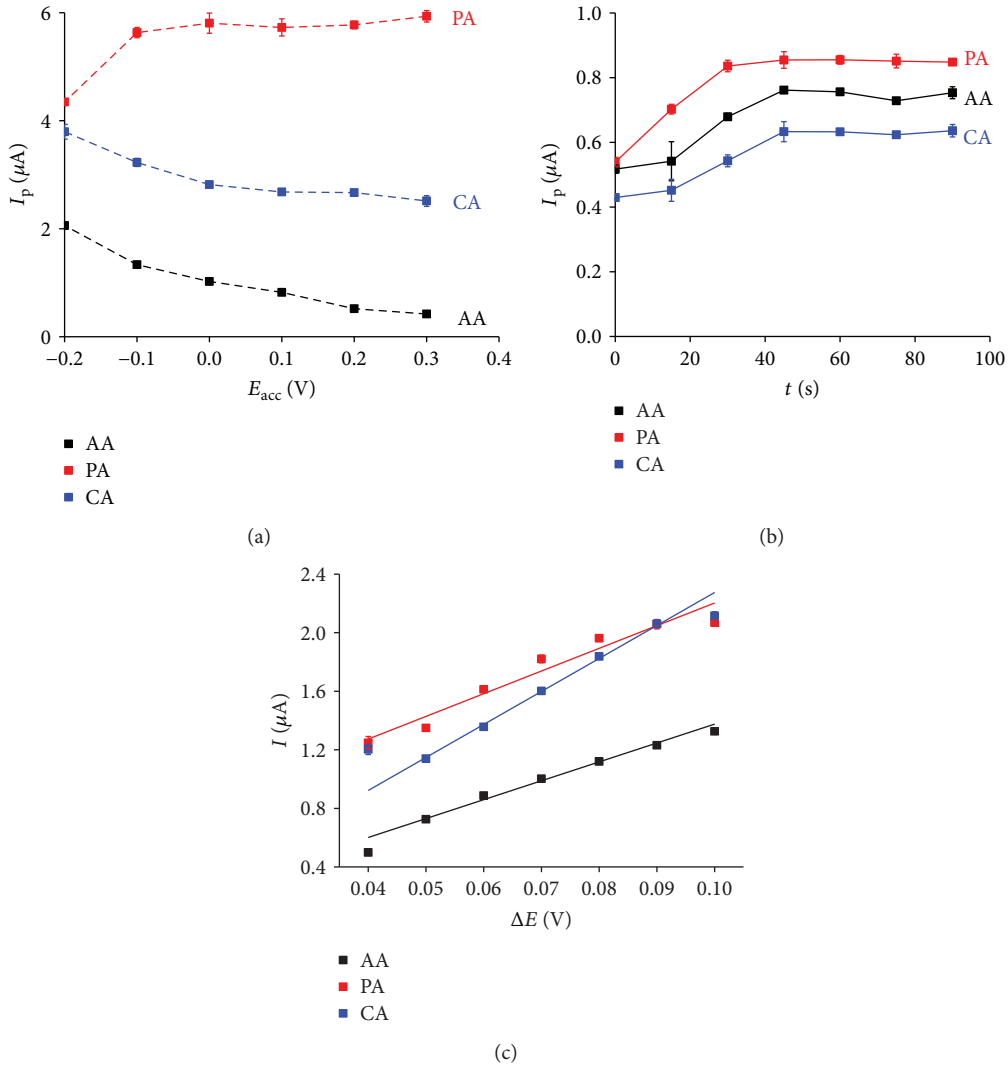

FIGURE 6: Dependence of I_p for AA, PA, and CA ($C_{AA} = C_{PA} = C_{CA} = 0.5\,\mu M$) in 0.2 M B–RBS of pH 3.2 on (a) accumulation potential, (b) accumulation time, and (c) pulse amplitude.

of −0.1 V was selected for AA, PA, and CA. The accumulation time also has an effect on the peak current. From Figure 6(b), it can be seen that I_p increases slightly with time and peaks at 45 s and then decreases afterwards. Therefore, 45 s was chosen as the accumulation time.

Pulse amplitudes significantly affect the voltammetric signal of the analytes. The pulse amplitude in the range of 0.04 V to 0.10 V was used in the DP-ASV method (Figure 6(c)). As seen in Figure 6(c), I_p increases linearly and E_p shifts negatively as the pulse amplitude increases. ΔE is larger than 0.06 V. The width of the current peak tends to be large, the peak resolution reduces, and the selectivity also reduces. The pulse amplitude of 0.06 V that provides a symmetric peak with low RSD (0.6%) was selected for the next experiments (Figure S3).

3.6. Effect of Interferents. The effect of the interferents on the anodic peak currents of AA, PA, and CA was estimated based on the relative error of the AA, PA, and CA when there is an interferent in the solution as opposed to its absence. Some possible interferents were investigated by adding them to a solution containing an equal concentration of AA, PA, and CA in the B–R buffer solution of pH 3.2 (5 μM). Inorganic cations including K^+, Na^+, Ca^{2+}, NH_4^+, CO_3^{2-}, NO_3^-, SO_4^{2-}, Cl^- with concentration ratios (interference compound : standard solution) of 1000 : 1 ÷ 3100 : 1 (mM/mM), and glutamic acid, benzoic acid, and glucose with concentration ratios in the range of 10 : 1 to 310 : 1 were tested as interferents (Tables S5–11). The analysis of the obtained responses made it possible to conclude that these compounds do not significantly interfere (<5%) in the determination of PA and CA under employed working conditions. However, dopamine and uric acid significantly affect the voltammetric signals of the analytes even when the molar ratio interferent : standard solution is equal to 1 : 10.

3.7. Repeatability, Linear Range, and Limit of Detection (LOD). The repeatability of ErGO/GCE for DP-ASV was estimated with different analyte concentrations. The DP-ASV

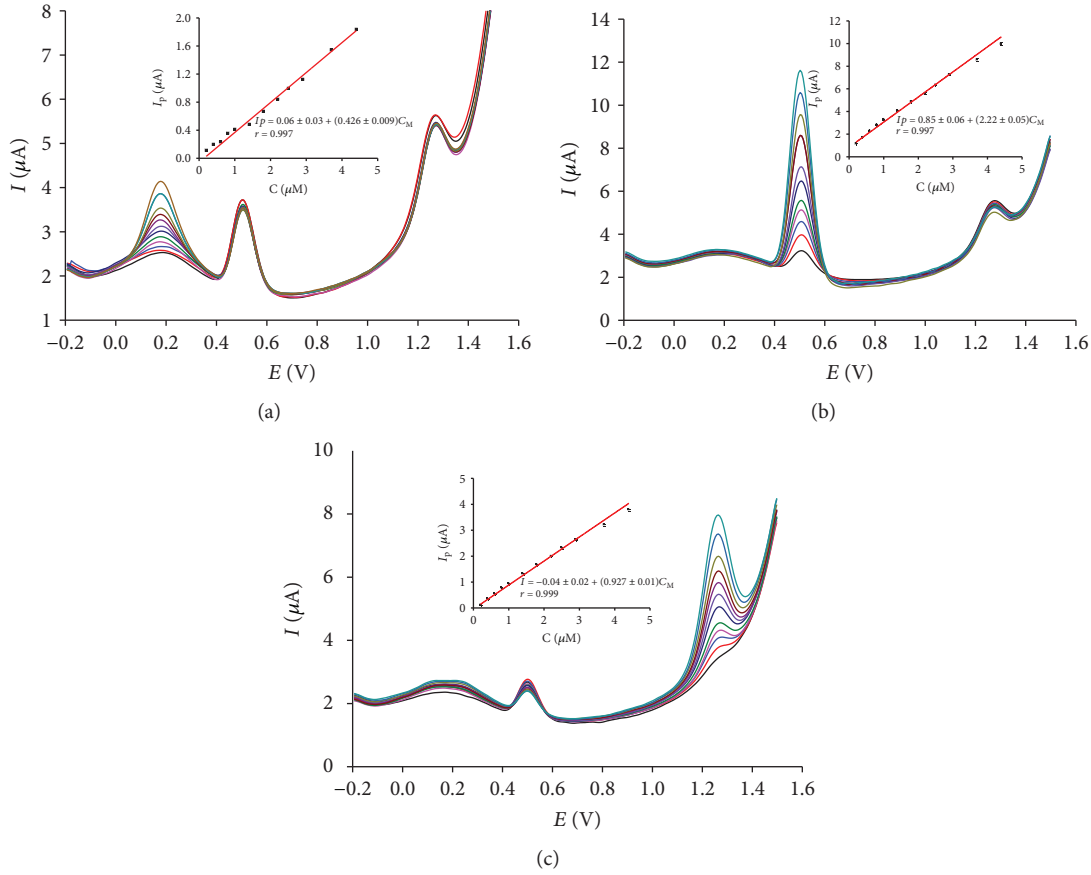

FIGURE 7: DP-ASV curves obtained on ErGO/GCE for (a) AA at different concentrations (0.2 to 4.4 μM) in the fixed concentrations of PA and CA ($C_{PA} = C_{CA} = 0.5\,\mu$M), (b) PA at different concentrations (0.2 to 4.4 μM) in the fixed concentrations of AA and CA ($C_{AA} = C_{CA} = 0.5\,\mu$M), and (c) CA at different concentrations (0.2 to 4.4 μM) in the fixed concentrations of AA and PA ($C_{AA} = C_{PA} = 0.5\,\mu$M).

curves were drawn to detect the mixtures of $C_{AA} = 100\,\mu$M, $C_{PA} = C_{CA} = 10\,\mu$M and $C_{AA} = 50\,\mu$M, $C_{PA} = C_{CA} = 5\,\mu$M and $C_{AA} = 10\,\mu$M, and $C_{PA} = C_{CA} = 1\,\mu$M, in which each signal was obtained by successive measurements for nine times (Figure S2). The obtained RSD is 0.76%, 1.00%, and 1.83% for $C_{AA} = 100\,\mu$M, $C_{PA} = 10\,\mu$M, and $C_{CA} = 10\,\mu$M, respectively; 1.28%, 3.03%, and 1.08% for $C_{AA} = 50\,\mu$M, $C_{PA} = 5\,\mu$M, and $C_{CA} = 5\,\mu$M, respectively; and 2.21%, 2.14%, and 2.35% for $C_{AA} = 10\,\mu$M, $C_{PA} = 1\,\mu$M, and $C_{CA} = 1\,\mu$M, respectively. These values are lower than 1/2 RSD_H [52]. Such reasonable RSD of the successive measurements indicates that ErGO/GCE can be repeatedly utilized for the detection of AA, PA, and CA in either low or high concentration range (Figure S4).

The individual determination of AA, PA, and CA was performed using the DP-ASV method, in which the concentration of one compound was raised while that of the other two was kept constant in the 0.2 M B–R buffer solution of pH 3.2 (Figure 7). As can be seen in the figure, the peak current of the two compounds with fixed concentration was fairly unchangeable while that of the third analyte rises with the increase of its concentration. This suggests that the oxidation reactions take place independently. The peak current increases in the concentration range from 0.2 μM to 4.4 μM. The linear regression equations are as follows:

$$\begin{aligned} I_{p,AA} &= 0.06 \pm 0.03 + (0.426 \pm 0.009) \cdot C_{AA}, \\ r &= 0.997, \\ p &< 0.001, \\ I_{p,PA} &= 0.85 \pm 0.06 + (2.22 \pm 0.05) \cdot C_{PA}, \\ r &= 0.997, \\ p &< 0.001, \\ I_{p,CA} &= -0.04 \pm 0.02 + (0.297 \pm 0.01) \cdot C_{CA}, \\ r &= 0.999, \\ p &< 0.001. \end{aligned} \tag{9}$$

In the range of 0.2 μM to 4.4 μM, the limit of detections (LOD) calculated using $3\sigma/s$ for AA, PA, and CA are 0.36, 0.25, and 0.23 μM, respectively.

The simultaneous determination of AA, PA, and CA was also conducted using the DP-ASV method. AA, PA, and CA were estimated simultaneously by increasing their concentrations in the 0.2 M B–R buffer solution of pH 3.2. Figure 8

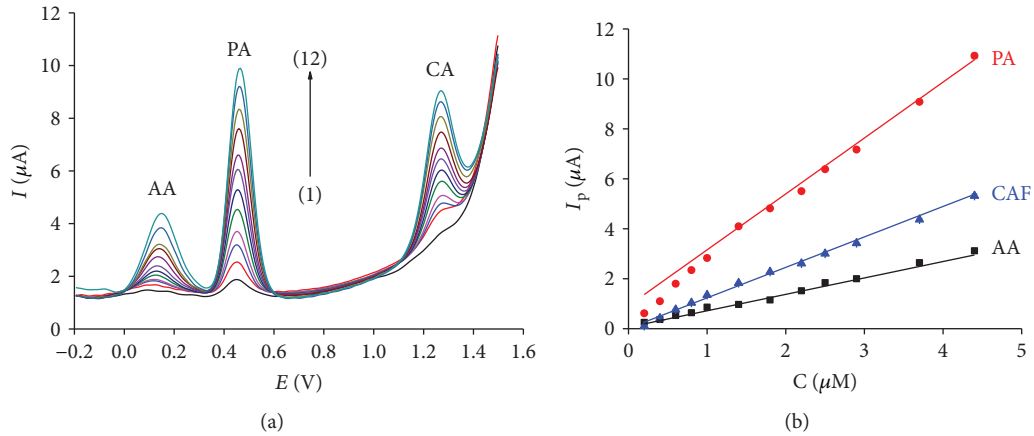

Figure 8: (a) DP-ASV curves obtained for the oxidation of AA, PA, and CA at equal concentrations in the 0.2 M B–R buffer solution of pH 3.2: (1) 0.2, (2) 0.4, (3) 0.6, (4) 0.8, (5) 1.0, (6) 1.4, (7) 1.8, (8) 2.2, (9) 2.5, (10) 2.9, (11) 3.7, and (12) 4.4 μM. (b) Linear plots of $I_{p,AA}$, $I_{p,PA}$, and $I_{p,CA}$ with their concentrations (scan rate = 0.02 V·s^{-1}; ΔE = 80 V; t_{acc} = 45 s; E_{acc} = −0.1 V).

presents the DP-ASV curves obtained for solutions containing an equal concentration of AA, PA, and CA in the range of 0.2 μM to 4.4 μM. The DP-ASV curves show oxidation peaks at around 0.16 V for AA, 1.25 V for PA, and 0.54 V for CA. The larger separation peak of the analyte favors simultaneous determination. The linear regression equations are expressed as follows:

$$\begin{aligned} I_{p,AA} &= 0.06 \pm 0.05 + (0.65 \pm 0.03) \cdot C_{AA}, \\ r &= 0.999, \\ p &< 0.001, \\ I_{p,PA} &= 1.0 \pm 0.1 + (2.23 \pm 0.09) \cdot C_{PA}, \\ r &= 0.997, \\ p &< 0.001, \\ I_{p,CA} &= 0.03 \pm 0.06 + (1.21 \pm 0.04) \cdot C_{CA}, \\ r &= 0.997, \\ p &< 0.001. \end{aligned} \tag{10}$$

In the range of 0.2 μM to 4.4 μM, the values of LOD were 0.30, 0.24, and 0.26 μM for AA, PA, and CA, respectively. It is noted that LOD of AA, PA, or CA in the simultaneous and individual determination is very close to each other. This, again, reaffirms that the oxidation of these compounds on the ErGO/electrode is independent. Hence, the simultaneous voltammetric determination of AA, PA, and CA is possible on ErGO/GCE in the mixed samples without any cross interference. This linearity is also acceptable for the simultaneous determination of AA, PA, and CA in pharmaceutical preparations, in which their amount is in the range of 100–200 mg, 200–500 mg, and 20–65 mg, respectively.

A comparison of the proposed method with other voltammetric methods for AA, PA, and CA determination is listed in Table 3. It could be noticed that LOD of AA, PA, and CA from the proposed method is lower or comparable with those results based on modified electrodes in previous papers [47, 49, 50, 52–58]. Overall, ErGO is proved to be an effective electrode modifier for the determination of AA, PA, and CA.

3.8. Real Sample Analysis. The proposed method was employed to determine the content of PA and CA in Panadol Extra, Hapacol Extra, and Tatanol (all of them are produced in Vietnam) and AA and PA in Effe Paracetamol, Ameflu C, and Efferalgan Vitamin C. Table 4 presents the amounts of AA, PA, and CA in the preparations with those determined using the HPLC method. The paired t-test was applied to these results. With the significant level $\alpha = 0.05$, the results show that the amounts of AA, PA, and CA determined with the proposed method found in pharmaceutical preparations are fairly close to the labeled amounts (AA: $t(2) = 3.78$, $p = 0.06$; PA: $t(5) = 2.05$, $p = 0.10$; and CA: $t(2) = 0.42$, $p = 0.71$). The results obtained with the proposed and HPLC methods are not statistically different (AA: $t(2) = 0.92$, $p = 0.45$; PA: $t(5) = -0.29$, $p = 0.78$; and CA: $t(2) = 1.22$, $p = 0.34$). Therefore, the precision of the determination was also found to be good. In these experiments, the concentrations of AA, PA, and CA were determined by means of standard addition method. The values of recovery of the spiked samples were conducted to evaluate matrix effects after the standard solution additions. The obtained results yielded good average recoveries, ranging from 96% to 108% for AA, 95% to 106% for PA, and 98% to 104% for CA suggesting that the present method does not suffer from any significant effects of matrix interference.

4. Conclusions

The present paper shows that the electrodeposition and electroreduction of graphene oxide using cyclic voltammetry have been successfully carried out on the glassy-carbon electrode. The modified electrode thereof can be used for the simultaneous determination of ascorbic acid, paracetamol, and caffeine. The results also reveal that the modified electrode exhibits high electrocatalytic activity towards the electrooxidation of ascorbic acid, paracetamol, and caffeine by

Table 3: Comparison of some figures of merit related to different electrodes for the determination of analytes.

Electrode	Method	Detection limit (μmol·L^{-1})			Reference numbers
		AA	PA	CA	
MWCNTs/GCE	SWV	0.01	—	0.0035	[56]
Carbon nanotubes/carbon–ceramic electrode	DPV	—	0.05	0.29	[57]
MWCNTs dispersed in polyhistidine/GCE	DPV	0.76	0.032	—	[58]
SWCNTs/carbon–ceramic electrode	DPV	3	0.12	—	[59]
Boron-doped diamond electrode	DPV	—	0.49	0.035	[60]
Flavonoid nanostructured/GCE	DPV	—	0.78	3.54	[61]
Boron-doped diamond film electrode	DPV	—	—	0.23	[62]
Gold-silver bimetallic nanotubes in a chitosan matrix/GCE	Amperometry	2	—	—	[63]
$MnFe_2O_4$@CNT-N/GCE		1.8	0.83	0.83	[64]
CuO-Gr/CPE	DPV	0.011	0.008	0.010	[65]
ErGO/GCE	DP-ASV	0.36	0.25	0.23	This work

Table 4: Results for AA, PA, and CA determination in pharmaceutical preparations and HPLC.

Pharmaceutical samples	Analytes	Labeled amounts (mg)	Methods	
			DP-ASV	HPLC
Panadol Extra	PA	500	496 ± 30	490 ± 1
	CA	65	65.3 ± 0.8	65.8 ± 0.5
Hapacol Extra	PA	500	498 ± 24	496.1 ± 0.9
	CA	65	64 ± 2	63.6 ± 0.1
Tatanol	PA	500	494 ± 3	492 ± 2
	CA	65	64 ± 1	63.7 ± 0.2
Effe Paracetamol	AA	200	194 ± 8	189 ± 1
	PA	200	201 ± 4	201 ± 2
Ameflu C	AA	100	98 ± 6	96.1 ± 0.9
	PA	500	495 ± 5	494 ± 3
Efferalgan Vitamin C	AA	200	197 ± 7	195 ± 2
	PA	330	331 ± 9	329 ± 4

enhancing the peak currents. Large peak separation between ascorbic acid and paracetamol could be obtained using DP-ASV, and this can facilitate their simultaneous and individual determination on the ErGO-modified glassy-carbon electrode. The excellent analytical performance and simple fabrication of ErGO make it a promising material for highly sensitive and selective electrochemical biosensors. Furthermore, the proposed method has been utilized for the simultaneous determination of ascorbic acid, paracetamol, and caffeine in pharmaceutical preparations with promising results.

Data Availability

The data used to support the findings of this study are available from the corresponding author upon request.

Conflicts of Interest

The authors declare that they have no conflicts of interest.

Acknowledgments

This work was supported by Project B2017–DHH–38 sponsored by the Ministry of Education and Training, Vietnam.

Supplementary Materials

Table S1 shows the order of experiments according to the Box–Behnken experimental design for AA. The rightmost column provides the values of peak current corresponding to each experiment. Table S2 shows the order of experiments according to the Box–Behnken experimental design for PA. The rightmost column provides the values of peak current corresponding to each experiment. Table S3 shows the order of experiments according to the Box–Behnken experimental design for CA. The rightmost column provides the values of peak current corresponding to each experiment. Table S4 presents estimated effects and coefficients of second-order polynomial equations. All the statistical and mathematical calculations were conducted using Minitab version 16. Table S5 shows that $NaNO_3$ does not interfere with the peak currents of AA, PA, and CA. Table S6 shows that K_2CO_3 does

not interfere with the peak currents of AA, PA, and CA. Table S7 shows that $CaCl_2$ does not interfere with the peak currents of AA, PA, and CA. Table S8 shows that $(NH_4)_2SO_4$ does not interfere with the peak currents of AA, PA, and CA. Table S9 shows that glucose does not interfere the peak currents of AA, PA and CA. Table S10 shows that glutamic acid does not interfere with the peak currents of AA, PA, and CA. Table S11 shows that benzoic acid does not interfere with the peak currents of AA, PA, and CA. Figure S1 presents CVs in in 1 mM $K_3[Fe(CN)_6]/K_4[Fe(CN)_6]$ at various scan rates to calculate the effective surface area of electrodes. Figure S2 presents the plot of the kinetic parameter ψ versus $\nu^{1/2}$ to obtain the heterogeneous electron transfer rate constant. Figure S3 shows DP-ASV curves using the pulse amplitude in the range of 0.04 V to 0.10 V. The pulse amplitude of 0.06 V provides a symmetric peak with low RSD (0.6%). Figure S4 represents the DP-ASV curves of AA, PA, and CA in which each signal was obtained by successive measurements for nine times. *(Supplementary Materials)*

References

[1] G. Hu, Y. Ma, Y. Guo, and S. Shao, "Electrocatalytic oxidation and simultaneous determination of uric acid and ascorbic acid on the gold nanoparticles-modified glassy carbon electrode," *Electrochimica Acta*, vol. 53, no. 22, pp. 6610–6615, 2008.

[2] J. Du, L. Shen, and J. Lu, "Flow injection chemiluminescence determination of epinephrine using epinephrine-imprinted polymer as recognition material," *Analytica Chimica Acta*, vol. 489, no. 2, pp. 183–189, 2003.

[3] E. L. Beard Jr., "The American Society of Health System Pharmacists," *JONA'S Healthcare Law, Ethics and Regulation*, vol. 3, no. 3, pp. 78-79, 2001.

[4] B. J. Sanghavi and A. K. Srivastava, "Simultaneous voltammetric determination of acetaminophen, aspirin and caffeine using an in situ surfactant-modified multiwalled carbon nanotube paste electrode," *Electrochimica Acta*, vol. 55, no. 28, pp. 8638–8648, 2010.

[5] T. Madrakian, E. Haghshenas, and A. Afkhami, "Simultaneous determination of tyrosine, acetaminophen and ascorbic acid using gold nanoparticles/multiwalled carbon nanotube/glassy carbon electrode by differential pulse voltammetric method," *Sensors and Actuators B: Chemical*, vol. 193, pp. 451–460, 2014.

[6] A. J. Jeevagan and S. A. John, "Electrochemical determination of caffeine in the presence of paracetamol using a self-assembled monolayer of non-peripheral amine substituted copper (II) phthalocyanine," *Electrochimica Acta*, vol. 77, pp. 137–142, 2012.

[7] A. Kriško, M. Kveder, and G. Pifat, "Effect of caffeine on oxidation susceptibility of human plasma low density lipoproteins," *Clinica Chimica Acta*, vol. 355, no. 1-2, pp. 47–53, 2005.

[8] J. Sawynok, "Pharmacological rationale for the clinical use of caffeine," *Drugs*, vol. 49, no. 1, pp. 37–50, 1995.

[9] U. L. Peri-Okonny, S. X. Wang, R. J. Stubbs, and N. A. Guzman, "Determination of caffeine and its metabolites in urine by capillary electrophoresis-mass spectrometry," *Electrophoresis*, vol. 26, no. 13, pp. 2652–2663, 2005.

[10] Q. Chen, Z. Guo, and J. Zhao, "Identification of green tea's (*Camellia sinensis* (L.)) quality level according to measurement of main catechins and caffeine contents by HPLC and support vector classification pattern recognition," *Journal of Pharmaceutical and Biomedical Analysis*, vol. 48, no. 5, pp. 1321–1325, 2008.

[11] B. Dejaegher, M. S. Bloomfield, J. Smeyers-Verbeke, and Y. Vander Heyden, "Validation of a fluorimetric assay for 4-aminophenol in paracetamol formulations," *Talanta*, vol. 75, no. 1, pp. 258–265, 2008.

[12] E. J. Llorent-Martínez, D. Šatínský, P. Solich, P. Ortega-Barrales, and A. Molina-Díaz, "Fluorimetric SIA optosensing in pharmaceutical analysis: determination of paracetamol," *Journal of Pharmaceutical and Biomedical Analysis*, vol. 45, no. 2, pp. 318–321, 2007.

[13] C. Akay, B. Gümüsel, T. Degim, S. Tartılmıs, and S. Cevheroglu, "Simultaneous determination of acetaminophen, acetylsalicylic acid and ascorbic acid in tablet form using HPLC," *Drug Metabolism and Drug Interactions*, vol. 15, no. 2-3, pp. 197–206, 1999.

[14] R. Thomis, E. Roets, and J. Hoogmartens, "Analysis of tablets containing aspirin, acetaminophen, and ascorbic acid by high-performance liquid chromatography," *Journal of Pharmaceutical Sciences*, vol. 73, no. 12, pp. 1830–1833, 1984.

[15] Sirajuddin, A. R. Khaskheli, A. Shah, M. I. Bhanger, A. Niaz, and S. Mahesar, "Simpler spectrophotometric assay of paracetamol in tablets and urine samples," *Spectrochimica Acta Part A: Molecular and Biomolecular Spectroscopy*, vol. 68, no. 3, pp. 747–751, 2007.

[16] P. Ortega Barrales, M. L. Fernández de Córdova, and A. Molina Díaz, "Indirect determination of ascorbic acid by solid-phase spectrophotometry," *Analytica Chimica Acta*, vol. 360, no. 1–3, pp. 143–152, 1998.

[17] M.-E. Capella-Peiró, D. Bose, M. F. Rubert, and J. Esteve-Romero, "Optimization of a capillary zone electrophoresis method by using a central composite factorial design for the determination of codeine and paracetamol in pharmaceuticals," *Journal of Chromatography B*, vol. 839, no. 1-2, pp. 95–101, 2006.

[18] X. Sun, Y. Niu, S. Bi, and S. Zhang, "Determination of ascorbic acid in individual rat hepatocyte by capillary electrophoresis with electrochemical detection," *Journal of Chromatography B*, vol. 870, no. 1, pp. 46–50, 2008.

[19] M. Blanco and M. Alcalá, "Simultaneous quantitation of five active principles in a pharmaceutical preparation: development and validation of a near infrared spectroscopic method," *European Journal of Pharmaceutical Sciences*, vol. 27, no. 2-3, pp. 280–286, 2006.

[20] P. Koblová, H. Sklenářová, I. Brabcová, and P. Solich, "Development and validation of a rapid HPLC method for the determination of ascorbic acid, phenylephrine, paracetamol and caffeine using a monolithic column," *Analytical Methods*, vol. 4, no. 6, p. 1588, 2012.

[21] Ľ. Švorc, J. Sochr, P. Tomčík, M. Rievaj, and D. Bustin, "Simultaneous determination of paracetamol and penicillin V by square-wave voltammetry at a bare boron-doped diamond electrode," *Electrochimica Acta*, vol. 68, pp. 227–234, 2012.

[22] L. Švorc, "Determination of caffeine: a comprehensive review on electrochemical methods," *International Journal of Electrochemical Science*, vol. 8, pp. 5755–5773, 2013.

[23] X. Zhu, J. Xu, X. Duan et al., "Controlled synthesis of partially reduced graphene oxide: enhance electrochemical determination of isoniazid with high sensitivity and stability," *Journal of Electroanalytical Chemistry*, vol. 757, pp. 183–191, 2015.

[24] L. Yang, D. Liu, J. Huang, and T. You, "Simultaneous determination of dopamine, ascorbic acid and uric acid at electrochemically reduced graphene oxide modified electrode," *Sensors and Actuators B: Chemical*, vol. 193, pp. 166–172, 2014.

[25] K. S. Novoselov, D. Jiang, F. Schedin et al., "Two-dimensional atomic crystals," *Proceedings of the National Academy of Sciences of the United States of America*, vol. 102, no. 30, pp. 10451–10453, 2005.

[26] K. S. Novoselov, Z. Jiang, Y. Zhang et al., "Room-temperature quantum hall effect in graphene," *Science*, vol. 315, no. 5817, article 1379, 2007.

[27] C. Lee, X. Wei, J. W. Kysar, and J. Hone, "Measurement of the elastic properties and intrinsic strength of monolayer graphene," *Science*, vol. 321, no. 5887, pp. 385–388, 2008.

[28] A. A. Balandin, S. Ghosh, W. Bao et al., "Superior thermal conductivity of single-layer graphene," *Nano Letters*, vol. 8, no. 3, pp. 902–907, 2008.

[29] L. Chen, Y. Tang, K. Wang, C. Liu, and S. Luo, "Direct electrodeposition of reduced graphene oxide on glassy carbon electrode and its electrochemical application," *Electrochemistry Communications*, vol. 13, no. 2, pp. 133–137, 2011.

[30] H. Wang, J. du, Z. Yao et al., "Facile fabrication, characterization of Pt–Ru nanoparticles modified reduced graphene oxide and its high electrocatalytic activity for methanol electrooxidation," *Colloids and Surfaces A: Physicochemical and Engineering Aspects*, vol. 436, pp. 57–61, 2013.

[31] G. Wang, J. Yang, J. Park et al., "Facile synthesis and characterization of graphene nanosheets," *Journal of Physical Chemistry C*, vol. 112, no. 22, pp. 8192–8195, 2008.

[32] S. Stankovich, R. D. Piner, X. Chen, N. Wu, S. T. Nguyen, and R. S. Ruoff, "Stable aqueous dispersions of graphitic nanoplatelets via the reduction of exfoliated graphite oxide in the presence of poly (sodium 4-styrenesulfonate)," *Journal of Materials Chemistry*, vol. 16, no. 2, pp. 155–158, 2006.

[33] X. Gao, J. Jang, and S. Nagase, "Hydrazine and thermal reduction of graphene oxide: reaction mechanisms, product structures, and reaction design," *The Journal of Physical Chemistry C*, vol. 114, no. 2, pp. 832–842, 2009.

[34] X. Liu, H. Kim, and L. J. Guo, "Optimization of thermally reduced graphene oxide for an efficient hole transport layer in polymer solar cells," *Organic Electronics*, vol. 14, no. 2, pp. 591–598, 2013.

[35] G. Williams, B. Seger, and P. V. Kamat, "TiO2-graphene nanocomposites. UV-assisted photocatalytic reduction of graphene oxide," *ACS Nano*, vol. 2, no. 7, pp. 1487–1491, 2008.

[36] S. Y. Toh, K. S. Loh, S. K. Kamarudin, and W. R. W. Daud, "Graphene production via electrochemical reduction of graphene oxide: synthesis and characterisation," *Chemical Engineering Journal*, vol. 251, pp. 422–434, 2014.

[37] E. Casero, A. M. Parra-Alfambra, M. D. Petit-Domínguez, F. Pariente, E. Lorenzo, and C. Alonso, "Differentiation between graphene oxide and reduced graphene by electrochemical impedance spectroscopy (EIS)," *Electrochemistry Communications*, vol. 20, pp. 63–66, 2012.

[38] N. M. Huang, "Simple room-temperature preparation of high-yield large-area graphene oxide," *International Journal of Nanomedicine*, vol. 6, pp. 3443–3448, 2011.

[39] A. Niazi, N. Khorshidi, and P. Ghaemmaghami, "Microwave-assisted of dispersive liquid–liquid microextraction and spectrophotometric determination of uranium after optimization based on Box–Behnken design and chemometrics methods," *Spectrochimica Acta Part A: Molecular and Biomolecular Spectroscopy*, vol. 135, pp. 69–75, 2015.

[40] S. M. Ghoreishi, H. Kamali, H. S. Ghaziaskar, and A. A. Dadkhah, "Optimization of supercritical extraction of linalyl acetate from lavender via Box-Behnken design," *Chemical Engineering and Technology*, vol. 35, no. 9, pp. 1641–1648, 2012.

[41] Y. Zhou, J. Z. Song, F. F. K. Choi et al., "An experimental design approach using response surface techniques to obtain optimal liquid chromatography and mass spectrometry conditions to determine the alkaloids in Meconopsi species," *Journal of Chromatography. A*, vol. 1216, no. 42, pp. 7013–7023, 2009.

[42] A. T. E. Vilian, V. Veeramani, S. M. Chen, R. Madhu, Y. S. Huh, and Y. K. Han, "Preparation of a reduced graphene oxide/poly-l-glutathione nanocomposite for electrochemical detection of 4-aminophenol in orange juice samples," *Analytical Methods*, vol. 7, no. 13, pp. 5627–5634, 2015.

[43] S. Cheemalapati, S. Palanisamy, and S.-M. Chen, "Electrochemical determination of isoniazid at electrochemically reduced graphene oxide modified electrode," *International Journal of Electrochemical Science*, vol. 8, pp. 3953–3962, 2013.

[44] Y. Shang, D. Zhang, Y. Liu, and Y. Liu, "Simultaneous synthesis of diverse graphene via electrochemical reduction of graphene oxide," *Journal of Applied Electrochemistry*, vol. 45, no. 5, pp. 453–462, 2015.

[45] H. Filik, G. Çetintaş, A. Aslihan Avan, S. N. Koç, and I. Boz, "Electrochemical sensing of acetaminophen on electrochemically reduced graphene oxide-nafion composite film modified electrode," *International Journal of Electrochemical Science*, vol. 8, pp. 5724–5737, 2013.

[46] Y. Xu, M. Gao, G. Zhang et al., "Electrochemically reduced graphene oxide with enhanced electrocatalytic activity toward tetracycline detection," *Chinese Journal of Catalysis*, vol. 36, no. 11, pp. 1936–1942, 2015.

[47] B. REZAEI and S. DAMIRI, "Voltammetric behavior of multi-walled carbon nanotubes modified electrode-hexacyanoferrate(II) electrocatalyst system as a sensor for determination of captopril," *Sensors and Actuators B: Chemical*, vol. 134, no. 1, pp. 324–331, 2008.

[48] D. A. C. Brownson, G. C. Smith, and C. E. Banks, "Graphene oxide electrochemistry: the electrochemistry of graphene oxide modified electrodes reveals coverage dependent beneficial electrocatalysis," *Royal Society Open Science*, vol. 4, no. 11, article 171128, 2017.

[49] M. Arvand and T. M. Gholizadeh, "Simultaneous voltammetric determination of tyrosine and paracetamol using a carbon nanotube-graphene nanosheet nanocomposite modified electrode in human blood serum and pharmaceuticals," *Colloids and Surfaces B: Biointerfaces*, vol. 103, pp. 84–93, 2013.

[50] L.'u. Švorc, P. Tomčík, J. Svítková, M. Rievaj, and D. Bustin, "Voltammetric determination of caffeine in beverage samples on bare boron-doped diamond electrode," *Food Chemistry*, vol. 135, no. 3, pp. 1198–1204, 2012.

[51] M. Li, X. Bo, Z. Mu, Y. Zhang, and L. Guo, "Electrodeposition of nickel oxide and platinum nanoparticles on electrochemically reduced graphene oxide film as a nonenzymatic glucose sensor," *Sensors and Actuators B: Chemical*, vol. 192, pp. 261–268, 2014.

[52] I. Taverniers, M. De Loose, and E. Van Bockstaele, "Trends in quality in the analytical laboratory. II. Analytical method validation and quality assurance," *TrAC Trends in Analytical Chemistry*, vol. 23, no. 8, pp. 535–552, 2004.

[53] R. S. Nicholson, "Theory and application of cyclic voltammetry for measurement of electrode reaction kinetics," *Analytical Chemistry*, vol. 37, no. 11, pp. 1351–1355, 1965.

[54] C. W. Foster, M. P. Down, Y. Zhang et al., "3D printed graphene based energy storage devices," *Scientific Reports*, vol. 7, article 42233, 2017.

[55] T. T. Minh, N. H. Phong, H. Van Duc, and D. Q. Khieu, "Microwave synthesis and voltammetric simultaneous determination of paracetamol and caffeine using an MOF-199-based electrode," *Journal of Materials Science*, vol. 53, no. 4, pp. 2453–2471, 2018.

[56] V. K. Gupta, A. K. Jain, and S. K. Shoora, "Multiwall carbon nanotube modified glassy carbon electrode as voltammetric sensor for the simultaneous determination of ascorbic acid and caffeine," *Electrochimica Acta*, vol. 93, pp. 248–253, 2013.

[57] B. Habibi, M. Jahanbakhshi, and M. Abazari, "A modified single-walled carbon nanotubes/carbon-ceramic electrode for simultaneous voltammetric determination of paracetamol and caffeine," *Journal of the Iranian Chemical Society*, vol. 11, no. 2, pp. 511–521, 2014.

[58] P. R. Dalmasso, M. L. Pedano, and G. A. Rivas, "Electrochemical determination of ascorbic acid and paracetamol in pharmaceutical formulations using a glassy carbon electrode modified with multi-wall carbon nanotubes dispersed in polyhistidine," *Sensors and Actuators B: Chemical*, vol. 173, pp. 732–736, 2012.

[59] B. Habibi, M. Jahanbakhshi, and M. H. Pournaghi-Azar, "Differential pulse voltammetric simultaneous determination of acetaminophen and ascorbic acid using single-walled carbon nanotube-modified carbon-ceramic electrode," *Analytical Biochemistry*, vol. 411, no. 2, pp. 167–175, 2011.

[60] B. C. Lourenção, R. A. Medeiros, R. C. Rocha-Filho, L. H. Mazo, and O. Fatibello-Filho, "Simultaneous voltammetric determination of paracetamol and caffeine in pharmaceutical formulations using a boron-doped diamond electrode," *Talanta*, vol. 78, no. 3, pp. 748–752, 2009.

[61] M. Amiri-Aref, J. B. Raoof, and R. Ojani, "A highly sensitive electrochemical sensor for simultaneous voltammetric determination of noradrenaline, acetaminophen, xanthine and caffeine based on a flavonoid nanostructured modified glassy carbon electrode," *Sensors and Actuators B: Chemical*, vol. 192, pp. 634–641, 2014.

[62] E. O. Faria, A. C. V. Lopes Junior, D. E. P. Souto et al., "Simultaneous determination of caffeine and acetylsalicylic acid in pharmaceutical formulations using a boron-doped diamond film electrode by differential pulse voltammetry," *Electroanalysis*, vol. 24, no. 5, pp. 1141–1146, 2012.

[63] P. Yang, X. Gao, L. Wang, Q. Wu, Z. Chen, and X. Lin, "Amperometric sensor for ascorbic acid based on a glassy carbon electrode modified with gold-silver bimetallic nanotubes in a chitosan matrix," *Microchimica Acta*, vol. 181, no. 1-2, pp. 231–238, 2014.

[64] D. M. Fernandes, N. Silva, C. Pereira et al., "MnFe 2 O 4@ CNT-N as novel electrochemical nanosensor for determination of caffeine, acetaminophen and ascorbic acid," *Sensors and Actuators B: Chemical*, vol. 218, pp. 128–136, 2015.

[65] Z. M. Khoshhesab, "Simultaneous electrochemical determination of acetaminophen, caffeine and ascorbic acid using a new electrochemical sensor based on CuO-graphene nanocomposite," *RSC Advances*, vol. 5, no. 115, pp. 95140–95148, 2015.